Supplementary Material

Boosting photocatalytic conversion of formic acid to CO over P-doped CdS

Pengfei Feng[a], Junhao Wu[a], Zimeng Fan[a], Baochun Ma[a], Yuanyuan Li [b] *, Xiangyu Meng[a, c] *, Yong Ding [a,d] *

[a] *State Key Laboratory of Applied Organic Chemistry, Key Laboratory of Advanced Catalysis of Gansu Province, College of Chemistry and Chemical Engineering, Lanzhou University, 222 Tianshui South Road, Lanzhou 730000, China*

[b] *Department of Biological and Chemical Engineering, Chongqing University of Education, No.9 Xuefu Avenue, Chongqing 400067, China*

[c] *Henan Provincial Key Laboratory of Nanocomposites and Applications, Institute of Nanostructured Functional Materials, Huanghe Science and Technology College, 666 Zijing Mountain South Road, Zhengzhou, 450006, China*

[d] *State Key Laboratory for Oxo Synthesis and Selective Oxidation, Lanzhou Institute of Chemical Physics, Chinese Academy of Sciences, 18 Tianshui Middle Road, Lanzhou 730000, China*

Table of content

1 Experiment

1.1 Equipment and apparatus

All chemicals were analytical, purchased from commercial sources and were utilized without any further purification. Pure water (18.2 MΩ cm, TOC < 3 ppb) was produced by Molecular Lab Water Purifier. Powder X-ray diffractions (XRD) were recorded on PANalytical X'Pert Pro Diffractometer using Cu–K radiation as the X-ray source. X-Ray photoelectron spectra (XPS) were measured by ESCALAB250xi with X-ray monochromatisation, in which the binding energy was calibrated using peak C 1s at 284.8 eV. UV-vis absorption spectra were registered in a TU-1810 spectrophotometer (Beijing Purkinje General Instrument Co., Ltd.) equipped with a photomultiplier tube detector. Diffuse reflectance spectra were measured using a PerkinElmer Lambda 950 UV-vis diffuse reflectance spectrophotometer. The surface morphology of the samples was characterized by a field emission scanning electron microscope (SEM, Carl Zeiss Ultra Plus, Germany) and transmission electron microscopy (TEM, FEI Tecnai G^2TF20, America). The amounts of H_2 and CO were detected by gas chromatography (GC) analysis.

1.2 Synthesis of CdS and P-doped CdS

The pure CdS photocatalyst was synthesized by a one-step hydrothermal method. 2.5 mmol cadmium chloride and 2.5 mmol sodium thiosulphate were added to 60 mL of deionized water, then a colorless clear solution was obtained by magnetic stirring at room temperature for half an hour. The solution was transferred to a stainless-steel autoclave lined with 100 mL of Teflon and reacted at 180 °C for 8 hours. After cooling to room temperature, centrifuging, wash the sample 3 times with anhydrous ethanol and deionized water and dry it in an oven at 60°C.

The synthesis procedure for phosphorus-doped CdS is similar to that of pure CdS. After dissolving 2.5 mmol of cadmium chloride and 2.5 mmol of sodium thiosulphate in 60 mL of deionized water to obtain a colorless clear solution, add 10, 15, 20 and 25 mmol of solid NaH_2PO_2 reagents, stir the solution magnetically at room temperature for half an hour. A colorless clear solution was obtained, then it was transferred to a stainless-steel autoclave with a 100 mL teflon liner and allowed to react at 180 °C for

8 hours. After cooling to room temperature, the sample was removed from reactor, centrifuged, washed three times with anhydrous ethanol and deionized water, respectively, and dried in an oven at 60 °C. The sample was named as P-CdS-X (X = 4, 6, 8 and 10). The number represents the molar ratio of sodium hypophosphite to sodium thiosulphate in the raw material.

1.3 Photocatalytic decomposition of formic acid

The preparation of the photocatalytic formic acid decomposition reaction solution is as follows: (1) In order to optimize the effect of acetonitrile content on the photocatalytic HCOOH decomposition activity, the pH value of HCOONa aqueous solutions were all adjusted to 3 by the HCOOH aqueous solutions of the same concentration, and then mixed with 0, 1, 3 and 5 times volume of acetonitrile. (2) For optimizing the pH of the reaction system, 4 M HCOOH aqueous was used to adjust the pH of an HCOONa aqueous solution to 2, 3, 4 and 5 while keeping the other conditions constant. (3) To test the effect of organic reagents on the photocatalytic activity of formic acid decomposition, the pH of HCOONa aqueous solution was adjusted to 3 with 4 M HCOOH aqueous solution and then mixed with three times the volume of acetonitrile (CH_3CN), dichloromethane (DCM), N, N-dimethylformamide (DMF) and dimethyl sulfoxide (DMSO).

Take 20 mL of the above reaction solution into the 80 mL photoreactor flask, then add 5 mg of CdS, P-CdS-4, P-CdS-6, P-CdS-8 and P-CdS-10 photocatalysts into the flask. Use ultrasonication for a few minutes to disperse the catalysts, and inject argon gas to replace the air in the flask. A 420 nm LED was selected as the excitation light source and photocatalytic formic acid decomposition reactions were conducted with agitation. Gas chromatography (Fuli GC9790Plus) with thermal conductivity detector (TCD) and hydrogen flame detector (FID) was used to determine the amount of gas products of formic acid decomposition.

1.4 EPR measurement

Electron paramagnetic resonance (EPR) spectroscopy was used to detect sulphur vacancy. 20 mg of the sample to be tested (CdS and P-CdS-8) was placed in a paramagnetic tube.

1.5 Photoeletrochemical measurement

Photoelectrochemical testing of the catalyst was carried out on the CHI760D electrochemical workstation. The electrolyte was 0.5M Na_2SO_4 aqueous solution. The standard three-electrode system consists of the working electrode FTO electrode (1 cm^2), the counter electrode Pt mesh and the reference electrode Ag/AgCl (3.5 M KCl, 0.208 V vs. NHE). The 5 mg sample was evenly dispersed in 1 mL of N, N-dimethylformamide (DMF) by ultrasonication, and then the resulting suspension and 0.5 % V/V Nafion solution were dropped successively onto the FTO glass. The working electrode was obtained after drying under infrared light. The photocurrent test was performed under a 300 W xenon lamp with a light intensity of 100 mW cm^{-1}.

2.Calculations

2.1 Data Calculation

Mass CO evolution rate of the sample was measured and calculated under experimental conditions.

Mass CO evolution rate = CO production amount ÷ (time × catalyst mass)

The photon flux of the incident light is measured using a photon flux meter.

2.2 Computational detail:

DFT calculations were conducted through the Vienna ab initio Simulation Package (VASP) with the projector augment wave method [1,2]. Generalized gradient approximation of the Perdew-Burke-Ernzerhof (PBE) functional was used as the exchange-correlation functional [3]. The Brillouin zone was sampled with 2 × 2 × 1 K points for surface calculation[4]. The cutoff energy was set as 500 eV, and structure relaxation was performed until the convergence criteria of energy and force reached 1 × 10^{-5} eV and 0.02 eV $Å^{-1}$, respectively. A vacuum layer of 15 Å was constructed to eliminate interactions between periodic structures of surface models. The van der Waals (vdW) interaction was amended by the zero damping DFT-D3 method of Grimme [5].

The adsorption energy (ΔE_{ads}) of HCOOH adsorption on surface is defined as

$$\Delta E_{ads} = E(*HCOOH) - E(*) - E(HCOOH)$$

where E(*HCOOH) and E(*) are the total energy of surface systems with and without HCOOH, respectively, E(HCOOH) is the energy of an isolated HCOOH. According to this definition, negative adsorption energy suggests that the adsorption process is exothermic and the adsorption system is thermodynamically stable. Contrarily, a positive value corresponds to an endothermic and unstable adsorption.

[1] G. Kresse, D. Joubert, Phys. Rev. B 59 (1999) 1758-1775.

[2] P.E. Blöchl, Phys. Rev. B 50 (1994) 17953-17979.

[3] J.P. Perdew, K. Burke, M. Ernzerhof, Phys. Rev. Lett. 77 (1996) 3865-3868.

[4] V. WANG, N. XU, J.-C. LIU, G. TANG, W.-T. GENG, VASPKIT: A User-Friendly Interface Facilitating High-Throughput Computing and Analysis Using VASP Code, Comput. Phy. Commun. 267, (2021) 108033.

[5] S. Grimme, S. Ehrlich, L. Goerigk, J. Comput. Chem. 32 (2011) 1456-1465.

3. Figures

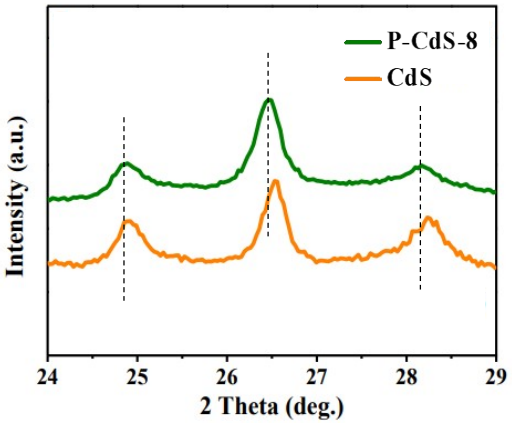

Fig. S1 Enlarged XRD images of CdS and P-CdS-8 photocatalysts.

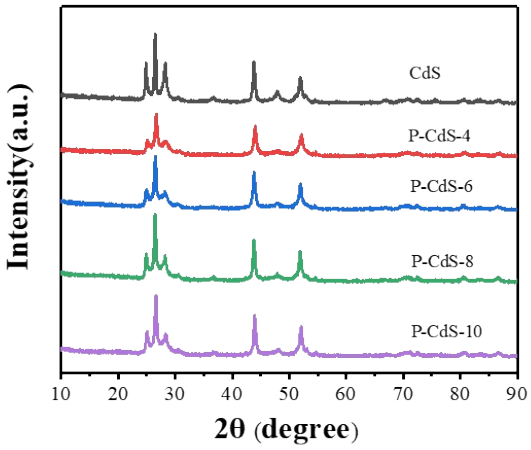

Fig. S2 XRD spectra of CdS and P-CdS-X samples.

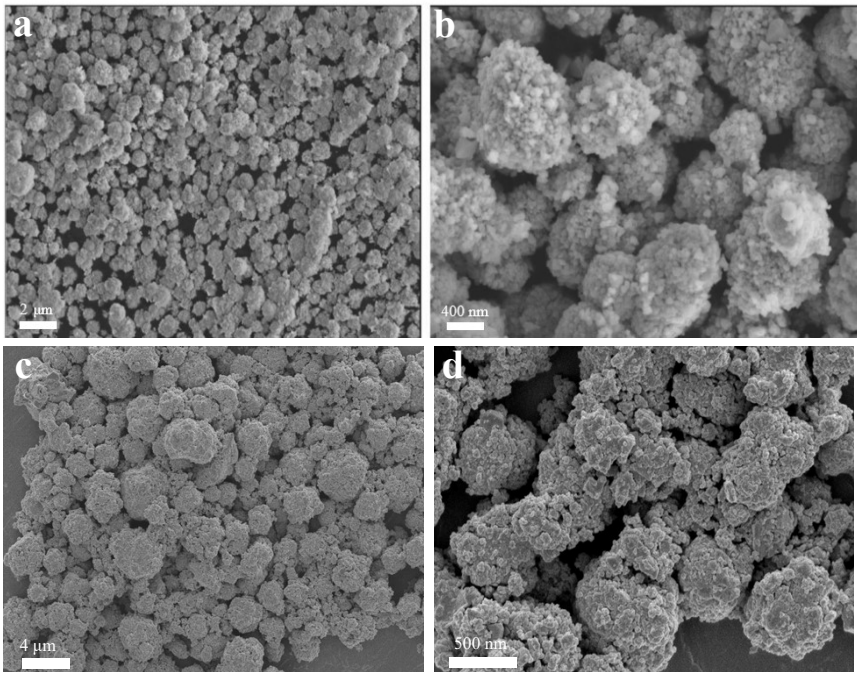

Fig. S3 SEM images of P-CdS-8 photocatalyst (a, b) and SEM images of CdS photocatalyst (c, d).

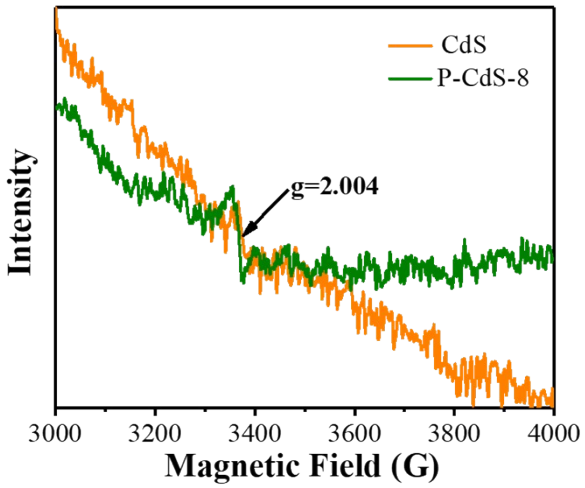

Fig. S4 EPR spectra of CdS and P-CdS-8 catalysts.

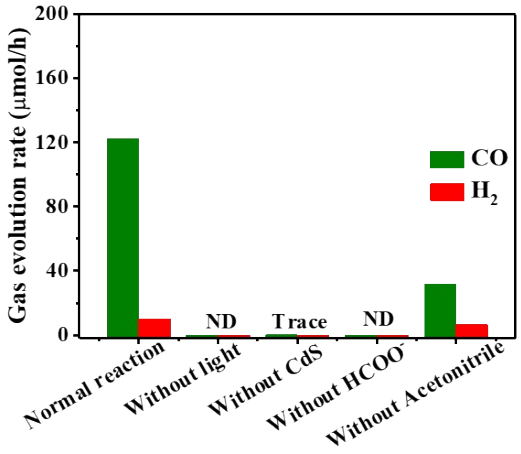

Fig. S5 Control experiments of P-CdS-8 photocatalyst. ND represents "not detected".

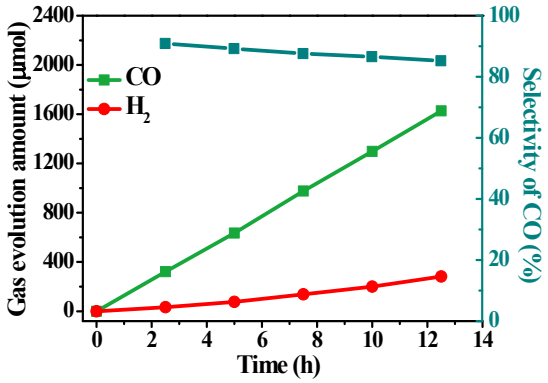

Fig. S6 Kinetical gas evolution curve of P-CdS-8 photocatalyst.

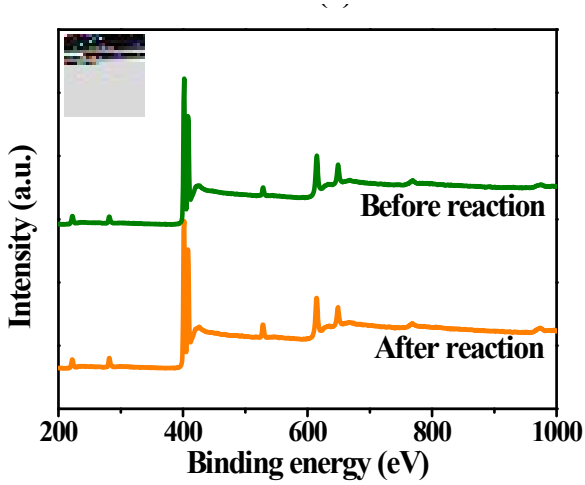

Fig. S7 XPS full spectrum of P-CdS-8 before and after photocatalytic reaction.

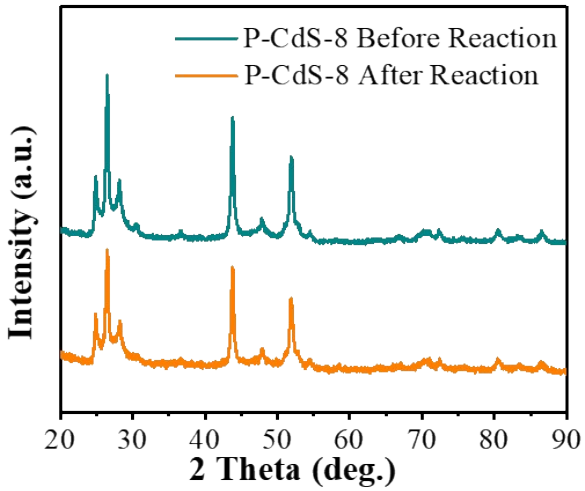

Fig. S8 XRD patterns of P-CdS-8 before and after the reaction.

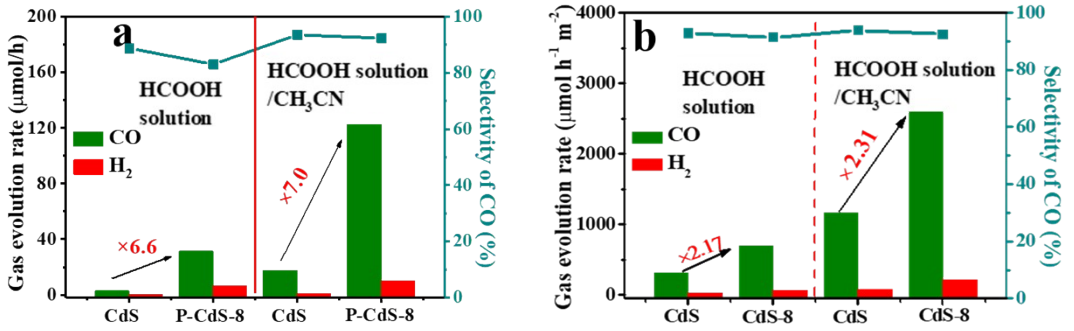

Fig. S9. Photocatalytic activity of CdS and P-CdS-8 without normalization(a) and after normalization(b).

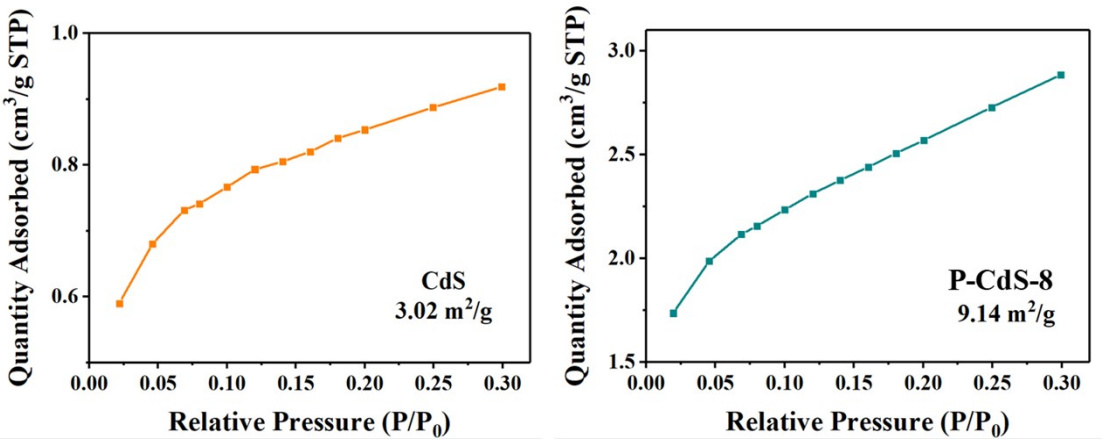

Fig. S10 Specific surface areas of CdS (a) and P-CdS-8 (b).

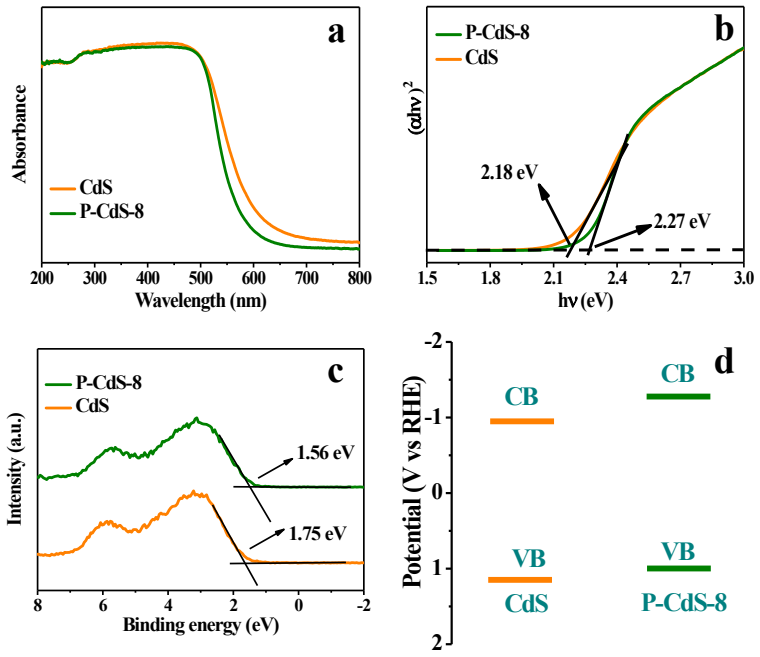

Fig. S11 UV-vis diffuse reflectance spectra (a), hv-$(\alpha hv)^2$ curves (b), XPS valence band spectra (c), band structure diagram (d) of CdS and P-CdS-8 photocatalysts.

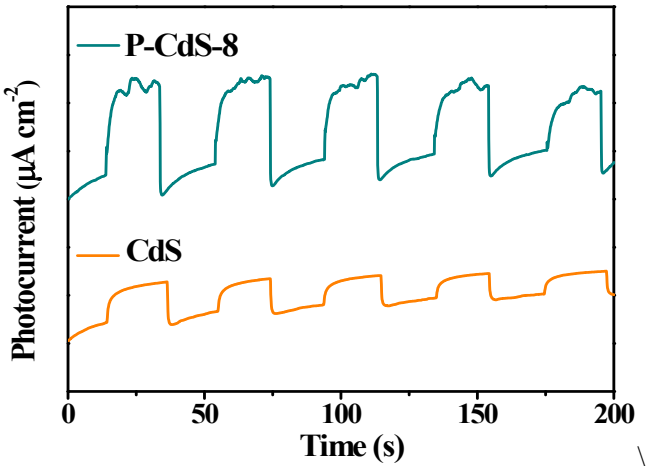

Fig. S12 Photocurrent response spectra of CdS and P-CdS-8 samples.

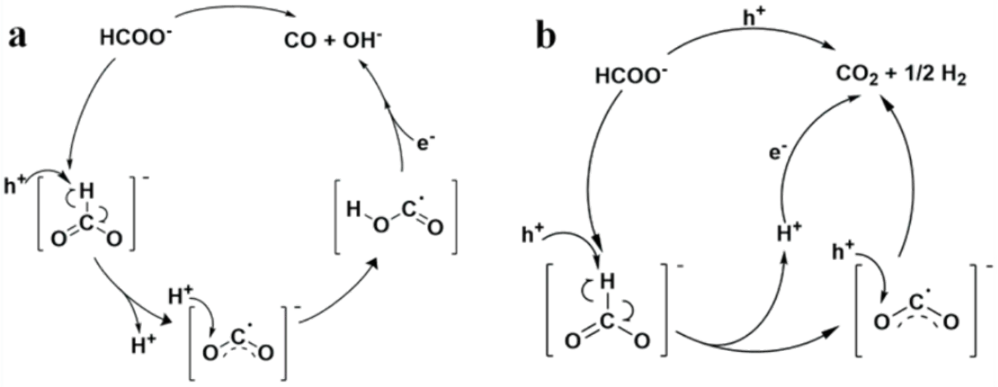

Fig. S13 Possible mechanism of CO (a)and H_2 (b)production from formate photocatalyzed by P-CdS-8.

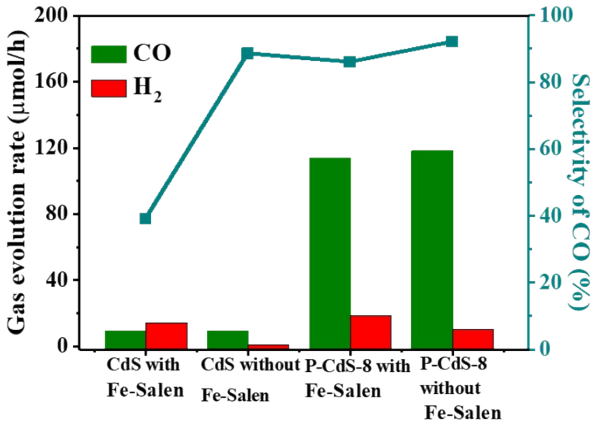

Fig. S14. Comparison of photocatalytic formic acid decomposition activities of CdS and P-CdS-8 with and without the addition of homogeneous molecular iron catalysts.

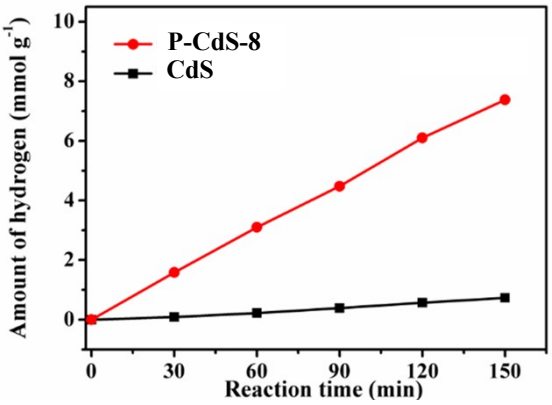

Fig. S 15. Photocatalytic hydrogen evolution activities of CdS and P-CdS-8 samples in Na_2S and Na_2SO_3 sacrificial reagent solution without adding formic acid.

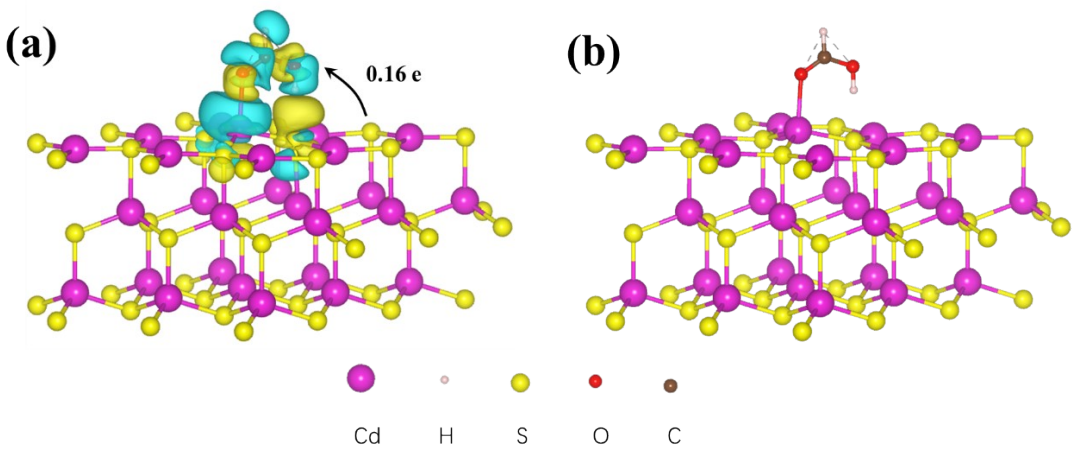

Fig. S16 Side view of (a) the charge density difference and (b) optimized structure of CdS (002) adsorbed with HCOOH with an isosurface of $5*10^{-4}$ e/Å^3. (The charge accumulation is shown as the yellow region, and the charge depletion is shown as the cyan region).

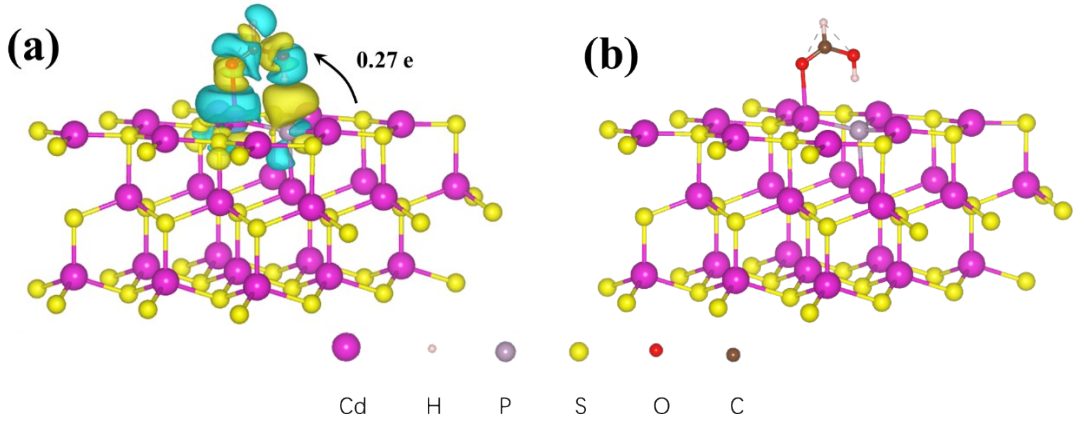

Fig. S17 Side view of (a) the charge density difference and (b) optimized structure of P-CdS (002) adsorbed with HCOOH with a isosurface of $5*10^{-4}$ e/Å^3. (The charge accumulation is shown as the yellow region, and the charge depletion is shown as the cyan region).

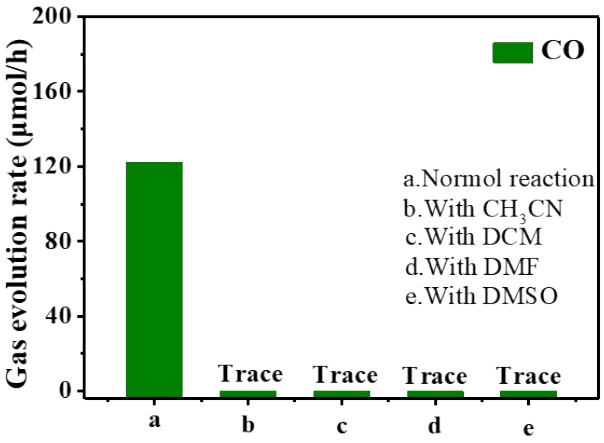

Fig. S18 Control experiments of P-CdS-8 photocatalyst. The experiment of entry b, c, d, and e were performed in CH_3CN, dichloromethane (DCM), N, N-dimethylformamide (DMF) and dimethyl sulfoxide (DMSO) in the absence of formic acid, respectively.

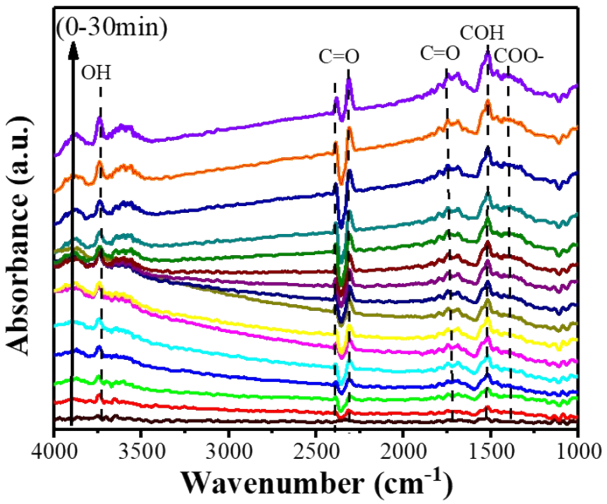

Fig. S19 In-situ FTIR spectroscopy of photocatalytic formic acid decomposition catalysed by P-CdS-8

Table S1. Comparison of photocatalysts for formic acid decomposition.

Photocatalyst	CO production rate (mmol g^{-1} h^{-1})	H_2 production rate (mmol g^{-1} h^{-1})	CO selectivity	H_2 selectivity	References
CdS	102		95		[1]
CdS/W_2N_3	103.5		-	-	[2]
CdS		150	-	-	[3]
CdS		278		100	[4]
Pd-C_3N_4		53.4		100	[5]
Pd@Au-NRs		10		100	[6]
AuPd-TiO_2		17.7		99.7	[7]
Au-TiO_2		3.9		90.7	[7]
Pt-CdS		0.85		83	[8]
Pd-Si		1.1		100	[9]
Pt-CdS		1.22			[10]
Ru-CdS/ZnS		5.85			[11]
hydrogenase-CdS	1.424		80		[12]
Au-La_2O_3/TiO_2		14.9			[13]
Pt-TiO_2		1.62			[14]
Rh-N:TiO_2		0.746		98	[15]
$RuCl_2(C_6H_6)]_2$ + 12 PPh_3		153.9			[16]
Bulk CdS		0.078			[17]
Pt-CdS NR		4.46			[18]
Ru-CdS@Al-HMS		0.541			[19]
P-CdS	24.5	2.02	92.4	7.6	This work

Table S2 The adsorption energy (ΔE_{ads}) of HCOOH adsorption on different catalyst surface

System	E(*)	E(HCOOH)	E(*HCOOH)	ΔE_{ads}（eV）
CdS (002)	-162.073	-29.8864	-192.624	-0.66451
P-CdS (002)	-162.541	-29.8864	-193.13	-0.70253

Reference

[1] M. F. Kuehnel, D. W. Wakerley, K. L. Orchard, E. Reisner, *Angew. Chem., Int. Ed.,* 2015, **54**, 9627-9631.

[2] T. Wang, M. Chen, J. Wu, P. Du, *J. Mater. Chem. A* 2023, **11**, 2246-2251.

[3] R. M. Irfan, T. Wang, D. Jiang, Q. Yue, L. Zhang, H. Cao, Y. Pan, P. Du, *Angew. Chem., Int. Ed.,* 2020, **59**, 14818-14824.

[4] T. Wang, L. Yang, D. Jiang, H. Cao, A. C. Minja, P. Du, *ACS Appl. Mater. Interfaces* 2021, **13**, 23751-23759.

[5] Y.-Y. Cai, X.-H. Li, Y.-N. Zhang, X. Wei, K.-X. Wang, J.-S. Chen, *Angew. Chem.* 2013, **125**, 12038-12041.

[6] Z. Zheng, T. Tachikawa, T. Majima, *J. Am. Chem. Soc.* 2015, **137**, 948-957.

[7] Z. Zhang, S.-W. Cao, Y. Liao, C. Xue, *Appl. Catal., B* 2015, **162**, 204-209.

[8] M. Matsumura, M. Hiramoto, T. Iehara, H. Tsubomura, *J. Phys. Chem. C* 1984, **88**, 248-250.

[9] K. Tsutsumi, N. Kashimura, K. Tabata, *Silicon* 2015, **7**, 43-48.

[10] Y. Li, L. Tang, S. Peng, Z. Li, G. Lu, *CrystEngComm* 2012, **14**, 6974-6982.

[11] X. Wang, W.-c. Peng, X.-y. Li, *Int. J. Hydrogen Energy* 2014, **39**, 13454-13461.

[12] A. I. Nedoluzhko, I. A. Shumilin, V. V. Nikandrov, *J. Phys. Chem. C* 1996, **100**, 17544-17550.

[13] M. Wu, M. Zhang, T. Lv, M. Guo, J. Li, C. A. Okonkwo, Q. Liu, L. Jia, *Appl. Catal., A* 2017, **547**, 96-104.

[14] Y. Li, F. He, S. Peng, D. Gao, G. Lu, S. Li, *J. Mol. Catal. A: Chem.* 2011, **341**, 71-76.

[15] G. Halasi, G. Schubert, F. Solymosi, *Catal. Lett.* 2012, **142**, 218-223.

[16] B. Loges, A. Boddien, H. Junge, J. R. Noyes, W. Baumann, M. Beller, *Chem. Commun.* **2009**, 4185-4187.

[17] I. Willner, Z. Goren, *J. Chem. Soc., Chem. Commun.* **1986**, 172-173.

[18] Y. Li, Y. Hu, S. Peng, G. Lu, S. Li, *J. Phys. Chem. C* 2009, **113**, 9352-9358.

[19] Y. J. Zhang, L. Zhang, S. Li, *Int. J. Hydrogen Energy* 2010, **35**, 438-444.